Polyoxometalates on Cationic Silica Nanoparticles. Physicochemical Properties of an Electrostatically Bound Multi-Iron Catalyst

Nelya M. Okun,[†] Michelle D. Ritorto,[†,‡] Travis M. Anderson,[†] Robert P. Apkarian,[‡] and Craig L. Hill*[,†]

Department of Chemistry, and Integrated Microscopy & Microanalytical Facility, Emory University, Atlanta, Georgia 30322

Received February 4, 2004. Revised Manuscript Received April 28, 2004

Reaction of a solution of the multi-iron polyoxometalate (POM) $K_9[(Fe^{III}(OH_2)_2)_3(A\text{-}\alpha\text{-}PW_9O_{34})_2]$ (K_9**1**) with a colloidal suspension of cationic silica nanoparticles ($(Si/AlO_2)Cl$) results in the production of a new heterogeneous oxidation catalyst (K_8**1**/(Si/AlO_2)). Dynamic light scattering data, coupled with elemental analysis and streaming potential measurements suggests that there are 58 molecules of POM electrostatically bound to the surface of each silica particle on average. Transmission electron microscopy confirms the presence of the POM on the surface of the cationic silica and shows the diameter of the $(Si/AlO_2)Cl$ and of the K_8**1**/(Si/AlO_2) nanoparticles to be ∼12 and ∼17 nm, respectively. Significantly, cryo-high-resolution scanning electron microscopy (cryo-HRSEM) shows that the POM retards the natural gelation process that colloidal silica is known to undergo upon aging. EPR and catalytic data collectively suggest that the exchange of the cationic silica for one of the nine K^+ cations associated with each POM is responsible for subtle structural changes in the POM which result in its activation as a catalyst.

Introduction

There are very few molecules or materials to date that catalyze rapid air-based oxidation under ambient conditions (1 atm of air and room temperature).[1,2] Such materials could facilitate the development of surfaces, fabrics (clothing, upholstery, etc.), and other formulations that purify the air without requiring energy sources (heat, light, etc.) or additives (solvents, activating agents, etc.). Recently, we reported the preparation of a new type of material that not only catalyzes the oxidation of sulfides and aldehydes but also does so efficiently under mild conditions.[2] This material consists of anionic metal−oxygen clusters (polyoxometalates or "POMs") that are electrostatically bound to cationic alumina-coated silica nanoparticles ($(Si/AlO_2)Cl$) (Figure 1). Specifically, the sandwich-type POM complex $K_9[(Fe^{III}(OH_2)_2)_3(A\text{-}\alpha\text{-}PW_9O_{34})_2]$ (K_9**1**) when bound to the surface of $(Si/AlO_2)^{n+}$ forms a heterogeneous catalyst

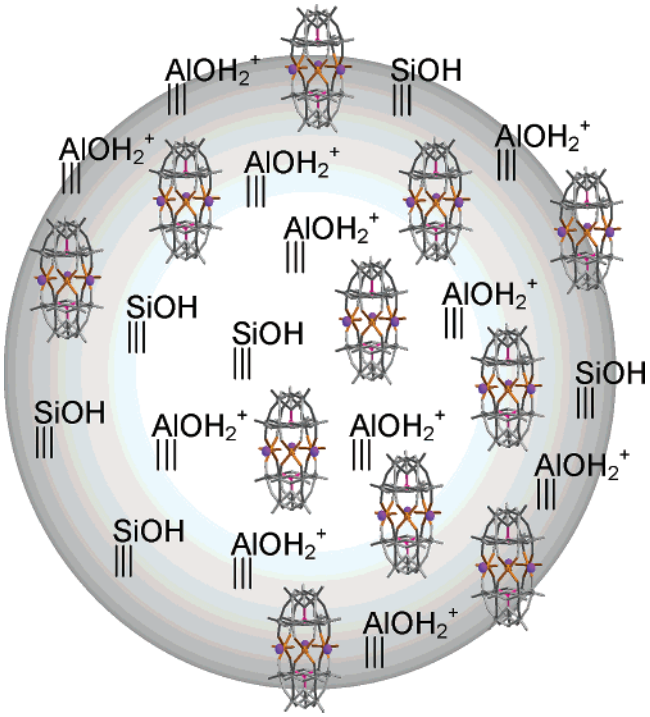

Figure 1. Representation of a single cationic silica nanoparticle with $[K_8(Fe^{III}(OH_2)_2)_3(A\text{-}\alpha\text{-}PW_9O_{34})_2]^-$ (K_8**1**; only the three K^+ cations intimately associated with the central Fe_3 unit are shown here) polyanion units electrostatically bound to the cationic alumina-coated surface $(SiAlO_2)^{n+}$. Assuming the nanoparticle is drawn to scale (7.3 cm = 17 nm), the K_8**1** monoanions are depicted in wireframe notation at nearly twice their actual size (0.9 × 1.5 cm = 1 × 2 nm) for clarity.

* To whom correspondence should be addressed.
[†] Department of Chemistry.
[‡] Integrated Microscopy & Microanalytical Facility.

(1) Representative recent work: (a) Bosch, E.; Kochi, J. K. *J. Org. Chem.* **1995**, *60*, 3172−3183. (b) Haruta, M. *Catal. Surv. Jpn.* **1997**, *1*, 61−73. (c) Xu, L.; Boring, E.; Hill, C. L. *J. Catal.* **2000**, *195*, 394−405. (d) Boring, E.; Geletii, Y. V.; Hill, C. L. *J. Am. Chem. Soc.* **2001**, *123*, 1625−1635. (e) Martin, S. E.; Rossi, L. I. *Tetrahedron Lett.* **2001**, *42*, 7147−7152. (f) Boring, E.; Geletii, Y. V.; Hill, C. L. *J. Mol. Catal.* **2001**, *176*, 49−63. (g) Rhule, J. T.; Neiwert, W. A.; Hardcastle, K. I.; Hill, C. L. *J. Am Chem. Soc.* **2001**, *123*, 12101−12102. (h) Okun, N. M.; Anderson, T. M.; Hill, C. L. *J. Mol. Catal. A* **2003**, *197*, 283−290. (i) Okun, N. M.; Anderson, T. M.; Hardcastle, K. I.; Hill, C. L. *Inorg. Chem.* **2003**, *42*, 6610−6612.
(2) Okun, N. M.; Anderson, T. M.; Hill, C. L. *J. Am. Chem. Soc.* **2003**, *125*, 3194−3195.

10.1021/cm049814v CCC: $27.50
Published on Web 06/05/2004

that is far more reactive than the same quantity of this same POM in solution.

The surface properties of hydrous oxides of aluminum, silicon, and iron and their interactions with dissolved metal salts or their complexes have been widely studied.[3−20] Initial models were based on the well-known double-electric layer theory and propose that the adsorption of species from solutions onto hydrous oxide surfaces may result solely from electrostatic interactions.[19] More recently, a surface complexation mechanism proposed that the sorbing ions react chemically with specific surface hydroxyl groups after approaching the interfacial electric field of the silica nanoparticle.[21] This model was subsequently developed into its various modern computational forms by many authors.[6] Although silicas containing cationic aluminum or iron oxide surfaces have been studied, there are few reports of interactions of these surfaces with negatively charged metal complexes such as POMs.[11−14,20,22−24] In separate but phenomenologically related work, catalytically active POMs[25,26] and methyltrioxorhenium[27] have been shown to associate with polyether-modified silica surfaces.

We report here a detailed study of the physicochemical properties of cationic aluminum hydroxide-coated silica nanoparticles ($(Si/AlO_2)Cl$) and their complexation with a multi-iron polyoxometalate (K_9**1**). Three techniques (elemental analysis, dynamic light scattering (DLS), and streaming potential measurements) are consistent with the conclusion that there are 58 ± 2 K_8**1** monoanions on average per cationic silica nanoparticle (one K^+ cation is lost upon binding of the POM to the cationic silica giving K_8**1**). Furthermore, both transmission electron microscopy (TEM) and DLS show the average diameter of $(Si/AlO_2)Cl$ particles to be ∼12 nm and that of K_8**1**/(Si/AlO_2) to be ∼17 nm. Cryo-high-resolution scanning electron microscopy (cryo-HRSEM) studies of colloidal suspensions of $(Si/AlO_2)Cl$ and K_8**1**/(Si/AlO_2) indicate that the presence of K_8**1** inhibits the aggregation and gelation of the $(Si/AlO_2)Cl$ upon aging. EPR studies show an increase in the intensity of a high-spin ferric signal at $g = 4.30$ as well as a minor change in shape, suggesting that the POM undergoes subtle changes upon binding to the cationic silica surface. Control experiments indicate that decomposition of the POM through the dissociation of the Fe(III) centers or isomerization to the B-type sandwich complex is not likely responsible for the pronounced enhancement seen in catalytic activity upon immobilization of the POM.

Experimental Section

General Procedures. $K_9[(Fe(OH_2)_2)_3)(A\text{-}\alpha\text{-}PW_9O_{34})_2]$ (K_9**1**) and $[(n\text{-}C_4H_9)_4N]_6[Fe_4(OH_2)_2(B-PW_9O_{34})_2]$ were prepared by the literature procedures and their purities were confirmed by FT-IR spectroscopy.[2,28] Bindzil CAT colloidal silica (herein designated "$(Si/AlO_2)Cl$") was obtained from Akzo Nobel and was further purified by diafiltration (VIVAscience VIVASPIN 20). The purified suspension was placed in an ultrasonic bath (Cole-Parmer Ultrasonic Cleaner) for 10 min to break up aggregates. K_8**1**/(Si/AlO_2) was prepared by the literature method.[2] FT-IR and DRIFT spectra were obtained on a Nicolet 510 FT-IR spectrometer. Dynamic light scattering (DLS) using a Coulter N4 Plus instrument provided the particle size distributions of $(Si/AlO_2)Cl$ and K_8**1**/(Si/AlO_2) (general conditions: 25 °C; diluent water; angle 90.0°; size distribution of particles (SDP) settings: min = 1.0 nm, max = 100 nm; number of bins = 31). BET surface area measurements of dry samples of $(Si/AlO_2)Cl$ and K_8**1**/(Si/AlO_2) were performed using a Quantachrome Nova 2000 surface area analyzer. Conductivities of silica samples were measured on a Fisher Scientific Conductivity Meter, Model 09-326-2. GC-MS was performed on a Hewlett-Packard 5890 Series II gas chromatograph connected to a Hewlett-Packard 5971 mass selective detector. GC was performed on a Hewlett-Packard 5890 gas chromatograph equipped with a 5% phenyl methyl silicone capillary column, flame ionization detector, and a Hewlett-Packard 3390A series integrator using N_2 as the carrier gas. Elemental analyses were performed by Desert Analytics, Tucson, AZ.

X-ray Powder Patterns. Samples of K_9**1** and K_8**1**/(Si/AlO_2) were finely ground and placed in glass capillaries. Various rotation frames were taken with a Bruker D8 X-ray diffractometer at 23 °C using a SMART 1000 CCD detector and monochromatic Mo Kα radiation. The sample was rotated about the φ axis during exposure and the frames were obtained at either 0° or −30° in 2θ and ω. The frames were processed and analyzed using GADDS software (Version 4.1.15, Bruker AXS, Inc., Madison, WI).

Titration Experiments. For acid−base titrations, colloidal suspensions (1 g) or dried samples (0.14 g) of $(Si/AlO_2)Cl$ and K_8**1**/(Si/AlO_2) were mixed with 25 mL of either 0.1 or 0.01 M NaCl, purged with Ar for 10 min to remove dissolved CO_2, and

(3) Iler, R. K. *The Chemistry of Silica*; John Wiley & Sons: New York, 1979.
(4) Bergna, H. E., Ed. *The Colloid Chemistry of Silica*; American Chemical Society: Washington, DC,1994.
(5) Lyklema, H. *Fundamentals of Interface and Colloid Science*; Academic Press: London, 2000; Vols. 1−3.
(6) Dzomback, D. A.; Morel, F. M. M. *Surface Complexation Modeling: Hydrous Ferric Oxide*; John Wiley & Sons: New York, 1990.
(7) (a) Hunter, R. J. *Foundations of Colloid Science*; Oxford University Press: New York, 1987; Vols. 1 and 2. (b) Hunter, R. J. *Introduction to Modern Colloid Science*; Oxford University Press: New York, 1993.
(8) Goloub, T. P.; Koopal, L. K.; Bijsterbosch, B. H. *Langmuir* **1996**, *12*, 3188−3194.
(9) Larson, I.; Attard, P. *J. Colloid Interface Sci.* **2000**, *227*, 152−163.
(10) Okada, K.; Tomita, T.; Kameshima, Y.; Yasumori, A.; MacKenzie, J. D. *J. Colloid Interface Sci.* **1999**, *219*, 195−200.
(11) Fraile, J. M.; Garcia, J. I.; Mayoral, J. A.; Pires, E.; Salvatella, L.; Ten, M. *J. Phys. Chem. B* **1999**, *103*, 1664−1670.
(12) Iengo, P.; Di Serio, M.; Sorrentino, A.; Solinas, V.; Santacesaria, E. *Appl. Catal., A* **1998**, *167*, 85−101.
(13) Legrand, A. P., Ed. *The Surface Properties of Silicas*; John Wiley & Sons: New York, 1998.
(14) Cativela, C.; Fraile, J. M.; Garcia, J. I.; Mayoral, J. A.; Pires, E.; Royo, A. J.; Figueras, F.; de Menorval, L. C. *Tetrahedron* **1993**, *49*, 4073−4084.
(15) Contescu, C.; Vass, M. I. *Appl. Catal.* **1987**, *33*, 259−271.
(16) van den Vlekkert, H.; Bousse, L.; de Rooij, N. *J. Colloid Interface Sci.* **1988**, *122*, 336−345.
(17) Sprycha, R. *J. Colloid Interface Sci.* **1989**, *127*, 1−11.
(18) Summers, J. C.; Ansen, S. A. *J. Catal.* **1978**, *52*, 445−452.
(19) Brunelle, J. P. *Pure Appl. Chem.* **1978**, *50*, 1211−1229.
(20) (a) Allen, L. H.; Mattijevic, E. *J. Colloid Interface Sci.* **1970**, *33*, 420−429. (b) Allen, L. H., Mattijevic, E. *J. Colloid Interface Sci.* **1969**, *31*, 287−296.
(21) Hohl, H.; Sigg, L.; Stumm, W. Characterization of Surface Chemical Properties of Oxides in Natural Waters. In *Particulates in Water*; Kavanaugh, M. C., Leckie, J. O., Eds.; Advances in Chemistry Series 189; American Chemical Society: Washington, DC, 1980; pp 1−31.
(22) Ermakova, L. E.; Sidorova, M. P.; Smirnov, V. M. *Kolloid. Zh.* **1997**, *59*, 563−565.
(23) Kuan, W. H.; Lo, S. L.; Wang, M. K. *Water Sci. Technol.* **2000**, *42*, 441−446.
(24) Rusmusson, M.; Wall, S. *Colloids Surf., A* **1997**, *122*, 169−181.
(25) Neumann, R.; Cohen, M. *Angew. Chem., Int. Ed. Engl.* **1997**, *36*, 1738−1740.
(26) Cohen, M.; Neumann, R. *J. Mol. Catal., A: Chem.* **1999**, *146*, 291−298.
(27) Neumann, R.; Wang, T. J. *J. Chem. Soc., Chem. Commun.* **1997**, *19*, 1915−1916.
(28) Zhang, X.; Chen, Q.; Duncan, D. C., Lachicotte, R. J.; Hill, C. L. *Inorg. Chem.* **1997**, *36*, 4381−4386.

titrated stepwise with 0.1 M solutions of NaOH and HCl in the pH range of 4−10 using an ORION 230A pH meter. The electrostatic adsorption of K_9**1** on $(Si/AlO_2)Cl$ was studied by streaming potential measurements performed with a particle charge detector PCD-02 (Muetek, Germany). A diluted colloidal suspension of $(Si/AlO_2)Cl$ (5 g in 100 mL of deionized water) was titrated with a solution of K_9**1** (0.005 M). Diluted colloidal suspensions of $(Si/AlO_2)Cl$ and K_8**1**$/(Si/AlO_2)$ (0.1 g in 140 mL of deionized water, pH 4.0) were also titrated with a 0.001 N polyelectrolyte solution of poly(vinyl sulfate, potassium salt) (Aldrich).

Transmission Electron Microscopy. Stock suspensions were prepared by sonicating dry powders of $(Si/AlO_2)Cl$ and K_8**1**$/(Si/AlO_2)$ in deionized water with a high-intensity horn (Sonics & Materials, Inc. Vibra-Cell VC-600) at room temperature for 30 min. A drop of the stock suspension was then placed on a carbon-coated 200-mesh copper grid (Electron Microscopy Sciences) and allowed to set for 5 min. The aqueous phase was wicked away with filter paper and the grids were dried in vacuo for at least 2 h prior to imaging. Micrographs were taken on a JEOL JEM-1210 transmission electron microscope equipped with a LaB_6 electron source operated at 90 kV.

Cryo-HRSEM. Stock colloidal suspensions of $(Si/AlO_2)Cl$ and K_8**1**$/(Si/AlO_2)$ (approximately 14 wt %) were purified by diafiltration as described above. Approximately 5−10 μL of the stock suspension was pipetted into 3-mm gold planchets (Balzers BU 012 130T). The samples were plunge frozen in ethane at its melting point (−183 °C) and the vitrified samples were stored in a slotted Teflon holder under liquid nitrogen (LN_2). A sample was transferred to and mounted on the pre-cooled (ca. −170 °C) GATAN CT-3500 cryo-stage held within the cryo-preparation chamber. The specimen was fractured with a pre-chilled blade and washed with LN_2. The dual stage shutters were closed to minimize frost contamination and the cryo-stage was transferred to a Denton DV-602 chromium coater. The stage was allowed to equilibrate in a vacuum of $\sim 10^{-7}$ Torr before the samples were etched (ice sublimation under high vacuum) to remove bulk water (vitreous ice). Upon equilibration, the shutters were opened and the stage was warmed to −105 °C for 15−20 min. At the end of the designated etching time, the shutters were closed and the stage was returned to a temperature of −170 °C. A 2-nm layer of Cr was then sputter-coated onto the specimen.[29,30] After Cr coating, the stage shutters were closed again, and the stage was transferred to the upper stage of the DS-130F field emission scanning electron microscope.[31,32] The shutters were re-opened and any ice contamination that had formed on top of the Cr film during transfer was removed through sublimation by warming the sample to −115 °C in the lens of the microscope ($\sim 10^{-7}$ Torr).[30] The specimen was allowed to equilibrate for 30 min at −115 °C before imaging. Micrographs were digitally collected (as 5 MB TIFF files) at an accelerating voltage of 25 kV in 16 s to reduce specimen radiation.

EPR Studies. EPR experiments were performed on the POM alone (K_9**1**) and POM-treated silica before catalysis (K_8**1**$/(Si/AlO_2)$). All samples contained a total of 0.2 mmol of POM. Each was sonicated with the above-mentioned horn in 2 mL of light mineral oil (Fisher Scientific) for a total of 25 min. After each 30-s interval of sonication, the samples were allowed to cool to ambient temperature. EPR spectra were recorded on a Brüker 200 spectrometer at 6 K with a microwave frequency of 9.655 GHz and a microwave power of 20 dB.

Catalytic Studies. In a typical experiment, 0.09 mmol (0.397 M) of THT, 0.875 mmol (0.35M) of dichlorobenzene (internal standard), and the amount of catalyst containing 0.0045 mmol of POM were stirred in 2.5 mL of CH_3CN in a 20-mL glass vial fitted with a PTFE septum under 1 atm of air at 75 °C. Aliquots were removed at intervals over a period of 120 h and the products were identified and quantified by GC-MS and GC, respectively.

Results and Discussion

Chemistry of Polyoxometalate Binding. The new POM nanoparticles (K_8**1**$/(Si/AlO_2)$) were prepared by stirring an aqueous solution of K_9**1** with an aqueous colloidal suspension of nonporous, amorphous cationic silica nanoparticles ($(Si/AlO_2)Cl$; Bindzil CAT).[2] BET surface area measurement revealed that dry $(Si/AlO_2)Cl$ has a surface area of 2.75 m^2/g, showing it is nonporous to N_2. After isolation of the dried K_8**1**$/(Si/AlO_2)$, the resulting solid was washed with several portions of CH_3CN to remove any unbound POM (K_9**1**). Unlike traditional anionic silicas that do not strongly bind POMs (simple washing readily displaces the POM), loss of K_9**1** is only seen during the first washing of the new material. After binding of the POM, there is no significant change in the weight percent of POM or the observed surface area of the nanoparticles. Three preliminary lines of evidence show that the POM has been bound to the surface of the cationic silica. First, DRIFT data show small differences in the spectra of $(SiAlO_2)Cl$ vs K_8**1**$/(Si/AlO_2)$ over the range of approximately 1100−600 cm^{-1}, indicating POM immobilization on the nanoparticle surface (inset Figure 2). However, the dominant peaks attributable to $(SiAlO_2)Cl$[33] obscure much of the detail of the characteristic frequencies exhibited by K_9**1**. If the spectrum of $(SiAlO_2)Cl$ is subtracted from that of K_8**1**$/(Si/AlO_2)$, however, the frequencies diagnostic of K_9**1** (Figure 2) are present and have shifted approximately 20 cm^{-1} for the P−O bands (1100−1000 cm^{-1} region) and from 15 to 40 cm^{-1} for the W−O bands (1000−700 cm^{-1} region). Second, elemental analysis of K_8**1**$/(Si/AlO_2)$ yields the appropriate ratio of Fe:P:W (3:2:18) and suggests the loss of one K^+ cation on average upon binding of K_9**1** to the surface of $(SiAlO_2)^{n+}$.[2] Finally, powder XRD is consistent with microcrystalline K_8**1** bound to the surface of the amorphous silica. The values and intensities of 2θ seen in the powder pattern of K_8**1**$/(Si/AlO_2)$ semiquantitatively match those of the powder pattern of the parent POM, K_9**1** (see Supporting Information).

Dynamic light scattering (DLS) experiments show an average diameter of ∼12 nm for the $(Si/AlO_2)Cl$ particles. An average diameter of ∼17 nm is seen for the K_8**1**$/(Si/AlO_2)$ particles (Figure 3), an increase in size that statistically averages to the formation of the molar equivalent of a monolayer of K_8**1** monoanions on the alumina-coated surface.[2] If the diameter of the particles and the mass of SiO_2 in 100 mL of colloidal silica suspension is known, the average number of K_8**1** monoanions electrostatically bound to the surface of the $(Si/AlO_2)^{n+}$ nanoparticles can be calculated.[34] For the ∼17 nm K_8**1**$/(Si/AlO_2)$ nanoparticles, the number of molecules of K_8**1** associated with a single particle is

(29) Apkarian, R. P. *Scan. Microsc.* **1994**, *8*, 289−301.
(30) Apkarian, R. P.; Caran, K. L.; Robinson, K. A. *Microsc. Microanal.* **1999**, *5*, 197−207.
(31) Apkarian, R. P. *54th Annu. Proc. Microsc. Soc. Am.* **1996**, 816−817.
(32) Apkarian, R. P.; Lee, S.; Keiper, J. *56th Annu. Proc. Microsc. Soc. Am.* **1998**, 258−259.
(33) Yuan, Q.; Ying, S. *Huadong Ligong Daxue Xuebao* **1998**, *24*, 526−531.
(34) With use of the above diameters and assuming the density of $(Si/AlO_2)Cl$ to be ∼2.2 g/cm^3 (the known density of amorphous, anhydrous, nonporous silica), the surface areas of $(Si/AlO_2)Cl$ and K_8**1**$/(Si/AlO_2)$ are found to be 227 and 160 m^2/g, respectively (see ref 4).

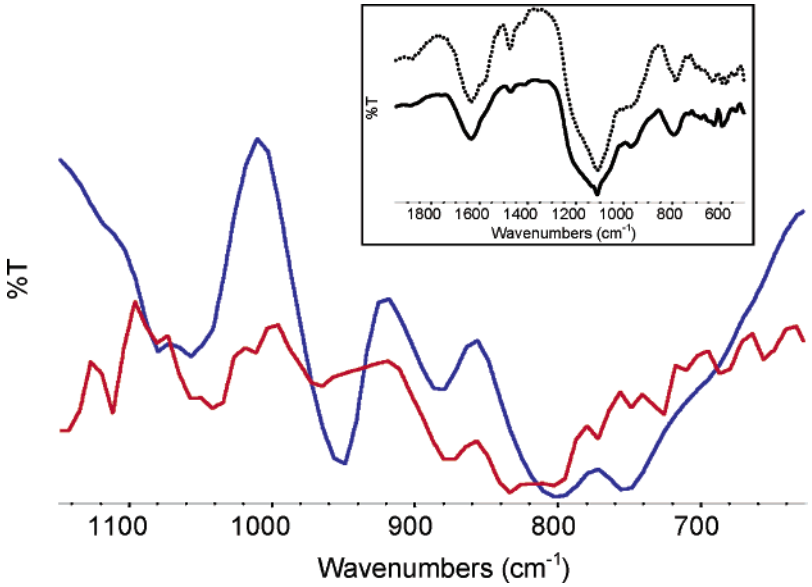

Figure 2. DRIFT spectra of $(Si/AlO_2)Cl$ and K_8**1**$/(Si/AlO_2)$ (inset; dotted and solid lines, respectively), the difference between $(Si/AlO_2)Cl$ and K_8**1**$/(Si/AlO_2)$ (red line), and K_9**1** (blue line). Small differences attributable to the electrostatic binding of the POM on cationic nanoparticles can be noted in the inset over the range of approximately 1100−600 cm^{-1}. Subtraction of the $(Si/AlO_2)Cl$ spectrum from the K_8**1**$/(Si/AlO_2)$ spectrum confirms the presence of POM and shows that these bands have shifted slightly.

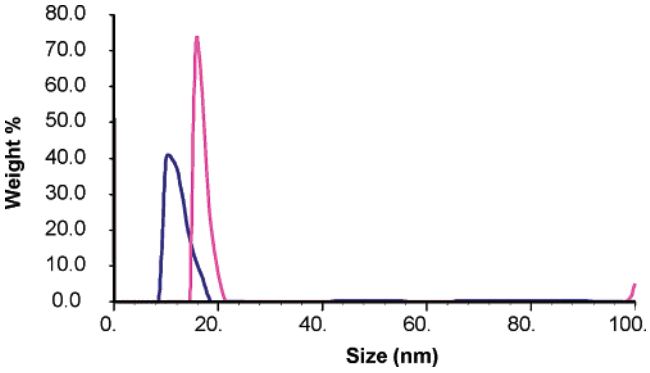

Figure 3. Dynamic light scattering (DLS) curves for $(Si/AlO_2)Cl$ (blue line) and K_8**1**$/(Si/AlO_2)$ (pink line). Approximately 95% of the $(Si/AlO_2)Cl$ particles ranges in size from 10.0 to 14.6 nm with an average diameter of ∼12 nm. The average diameter of K_8**1**$/(Si/AlO_2)$ particles increases to ∼17 nm with 95% of the particles falling in the range of 15.8 to 18.5 nm.

found to be 58 ± 2 (see Supporting Information). Elemental analysis of K_8**1**$/(Si/AlO_2)$ is consistent with this calculation.[2]

Titration Studies. The surface charges of cationic silica, $(Si/AlO_2)Cl$, and POM-coated silica, K_8**1**$/(Si/AlO_2)$, were determined using aqueous acid−base titrations.[22,23,35−37] Figure 4 shows the resulting titration curves for both colloidal suspensions (Figure 4A) and dried samples (Figure 4B). The charge densities (σ) are determined by eq 1,

$$\sigma = F\,[\Gamma_H - \Gamma_{OH} + \Sigma(z_M\Gamma_M) - \Sigma(z_A\Gamma_A)] \qquad (1)$$

where σ is the charge density (C/g), F is the Faraday constant (96458 C/mol), z is the valence of a sorbing ion,

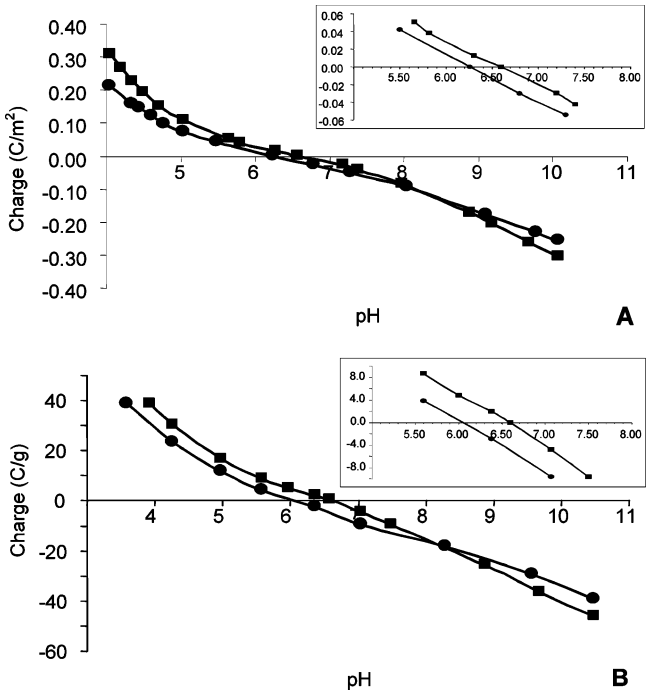

Figure 4. Point of zero charge (pzc) determinations for $(Si/AlO_2)Cl$ and K_8**1**$/(Si/AlO_2)$ as (A) colloidal suspensions or (B) dry powders. The surface charge of $(Si/AlO_2)Cl$ and K_8**1**$/(Si/AlO_2)$ as a function of pH are indicated by symbols ■ and ●, respectively. Conditions: 25 °C; 1 atm of Ar; K_8**1** = $K_8[(Fe^{III}(OH_2)_2)_3(A\text{-}\alpha\text{-}PW_9O_{34})_2]^{-}$; colloidal suspensions (1 g) or dry powders (0.14 g) were suspended in 25 mL of 0.1 M NaCl. The pzc of $(Si/AlO_2)Cl$ is 6.60 ± 0.005. The pzc of K_8**1**$/(Si/AlO_2)$ shifts to lower values due to the presence of K_8**1** monoanions on the cationic surface of the nanoparticle. A change of 0.36 and 0.55 pH units is seen for the colloidal suspension and the dried sample, respectively (see insets).

Γ_H and Γ_{OH} are the sorption densities (mol/g) of protons and hydroxide ions, and Γ_M and Γ_A are the sorption densities of specifically sorbed cations and anions, respectively. The sorption of anions on the surface of

(35) Bolt, G. H. *J. Phys. Chem.* **1957**, *61*, 1166−1169.
(36) Parks, G. A.; de Bruyn, P. L. *J. Phys. Chem.* **1962**, *66*, 967−973.
(37) Helmy, A. K.; Ferreiro, E. A.; Bussetti, S. G. *Z. Phys. Chem. (Leipzig)* **1980**, *261*, 1065−1073.

the cationic silica is expected to make σ more negative as the amount of POM on the surface increases. The point of zero charge (pzc) of alumina-modified silica depends on the amount of surface covered. It may vary from pH = 2 for conventional silica to pH = 8.5 for silica which is 100% covered by alumina.[22,23] According to the data presented in Figure 4, the pzc of $(Si/AlO_2)Cl$ is pH = 6.60 ± 0.005. This suggests that the surface of the Bindzil CAT is not completely covered with the positively charged aluminum oxide species. Consequently, there is a nonuniform distribution of charge on the surface. The shift in pH of the pzc to lower values for K_8**1**$/(Si/AlO_2)$ (0.36 and 0.55 pH units for the colloidal suspension and the dried sample, respectively) confirms the interaction of the negatively charged K_8**1** anions with the surface of the nanoparticles (insets Figure 4). This change in pH of the pzc is quantitatively related to the amount of K_8**1** specifically absorbed on the solid surface. There is less of a change seen in pH in the colloidal sample than in the dried sample. This is due to the fact that in the colloidal sample the POM is not in direct contact with the surface of the cationic nanoparticle, but instead is found in the anionic double electric layer that surrounds each particle in suspension. In the dried sample, the double electric layer is no longer present and the POM now rests directly on the cationic surface of the nanoparticle. The molecular representation and interpretation of the former and latter are solvent-separated and contact POM-counterion ion pairs, species recently probed and quantified for redox-active POMs using an ensemble of physical methods.[38,39]

The electrostatic adsorption of K_9**1** on the $(Si/AlO_2)^{n+}$ surface was also studied by streaming potential titrations. The streaming potential difference, E, is the potential difference at zero current caused by the flow of liquid under a pressure gradient through a membrane, plug, or capillary.[5] The streaming potentials of colloidal suspensions of $(Si/AlO_2)Cl$ and K_8**1**$/(Si/AlO_2)$ as a function of the volume of the polyelectrolyte poly(vinyl sulfate) (PVSK) are shown in Figure 5. The absorption of the polyanion K_9**1** on the surface of $(Si/AlO_2)^{n+}$ reduces the amount of positive charge and consequently decreases the amount of PVSK required to achieve a neutral charge. As shown in Figure 5, 1.2 mL less of PVSK is required to neutralize the charge of K_8**1**$/(Si/AlO_2)$ relative to $(Si/AlO_2)Cl$. This is consistent with the presence of 56 ± 2 molecules of K_8**1** per cationic silica nanoparticle (see Supporting Information for calculations).

Finally, a titration of a colloidal suspension of $(Si/AlO_2)Cl$ with a solution of K_9**1** (Figure 6) shows that when 0.035 mmol of K_9**1** is added to 5.0 g of $(Si/AlO_2)Cl$, the streaming potential drops from an initial value of 815 ± 1 to 0 ± 1 mV. After this charge neutralization is achieved, the addition of 0.0025 mmol more of K_9**1** makes the surface slightly negatively charged. This suggests that, after the equivalence point, the negatively charged K_9**1** molecules become the potential-determining anions. Calculations show that the

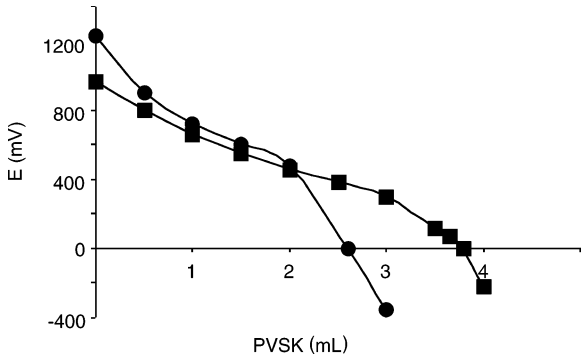

Figure 5. Streaming potential-polyelectrolyte titration curves. Streaming potential differences (E) of $(Si/AlO_2)Cl$ and K_8**1**(Si/AlO_2) suspensions as a function of the amount of potassium poly(vinyl sulfate) (PVSK) added are indicated by symbols ■ and ●, respectively. Conditions: 25 °C; 1 atm of Ar; K_8**1** = $K_8[(Fe^{III}(OH_2)_2)_3(A\text{-}\alpha\text{-}PW_9O_{34})_2]^{-}$; [PVSK] = 0.001 M; colloidal silica (0.5 mL) was suspended in 140 mL of water. The data show that there are 56 ± 2 molecules of K_8**1** per $(Si/AlO_2)Cl$ particle (see Supporting Information for calculations).

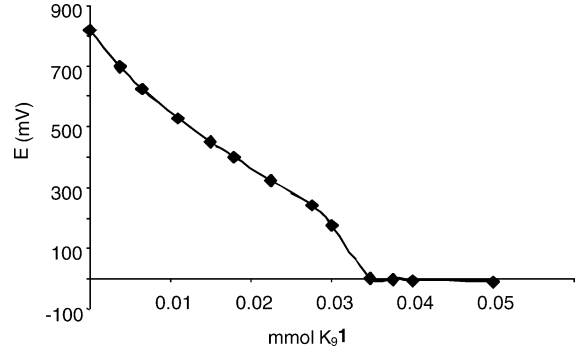

Figure 6. Streaming potentials as a function of K_9**1** added. Conditions: 25 °C; 1 atm of air; colloidal suspension of $(Si/AlO_2)Cl$ (5.5 g) in 100 mL of water was titrated with 0.005 M K_9**1**. A total of 0.035 mmol of K_9**1** is necessary to neutralize the surface of $(Si/AlO_2)^{n+}$. This corresponds to 57 ± 2 molecules of K_8**1** per cationic silica particle (see Supporting Information for calculations).

0.035 mmol of K_9**1** necessary to neutralize the surface of $(Si/AlO_2)Cl$ corresponds to approximately 57 ± 2 molecules of K_8**1** per cationic silica nanoparticle (see Supporting Information for calculations).

Electron Microscopy. *Transmission Electron Microscopy.* TEM was used to confirm the presence of K_8**1** on the surface of the $(Si/AlO_2)^{n+}$ nanoparticles and to determine the relative particle sizes of $(Si/AlO_2)Cl$ and K_8**1**$/(Si/AlO_2)$ (Figure 7). Several $(Si/AlO_2)Cl$ particles can be seen in Figure 7A as light gray spheres that are measured to be approximately 12 nm in diameter (indicated by arrows). Out of the eight representative particles shown, six of these (or 75%) fall in the 10−12 nm size range. This is in close agreement with the DLS data which indicate 77.8% of the $(Si/AlO_2)Cl$ particles have a diameter within this range.[2] Figure 7B shows a single $(Si/AlO_2)Cl$ particle at high magnification (760000×). K_8**1**$/(Si/AlO_2)$ particles are evident as dark gray spheres measured to be ∼17 nm in diameter in Figure 7C.[40a] Magnification of a single K_8**1**$/(Si/AlO_2)$ particle reveals black spots on the surface of the dark gray $(Si/AlO_2)^{n+}$ nanoparticle (Figure 7D). These high-electron-density regions (black areas) can be attributed to our W-based POM (K_8**1** monoanions) electrostatically bound to the surface of the

(38) Grigoriev, V. A.; Hill, C. L.; Weinstock, I. A. *J. Am. Chem. Soc.* **2000**, *122*, 3544−3545.
(39) Grigoriev, V. A.; Cheng, D.; Hill, C. L.; Weinstock, I. A. *J. Am. Chem. Soc.* **2001**, *123*, 5292−5307.

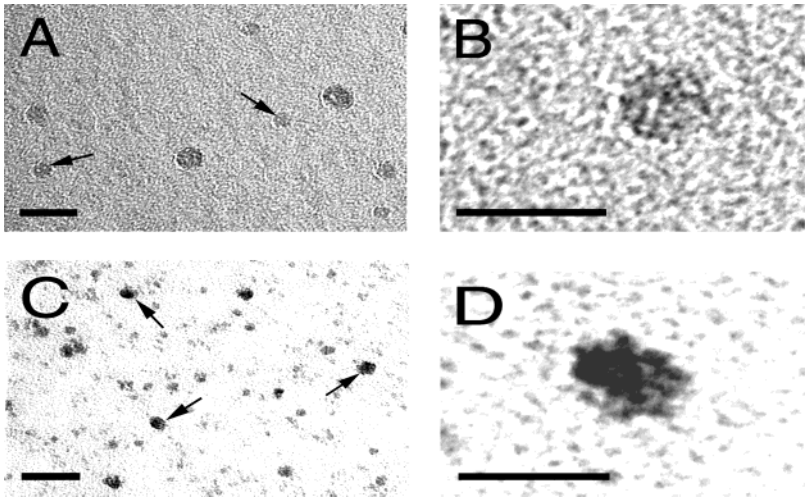

Figure 7. Transmission electron micrographs of cationic silica and POM electrostatically bound to cationic silica. (A) Global view (150000×) of $(Si/AlO_2)Cl$ nanoparticles. Bar = 50 nm. The particles appear as light gray spheres whose borders are difficult to discern from the carbon coating on the grid due to the similarity in their electron densities. Representative $(Si/AlO_2)Cl$ nanoparticles falling in the 10−12 nm range, the size range consistent with DLS measurements, are indicated by arrows. (B) Enlargement of a single $(Si/AlO_2)Cl$ particle allows for clear determination of its size (∼12 nm). Bar = 25 nm. (C) Global view (150000×) of K_8**1**$/(Si/AlO_2)$ nanoparticles. Bar = 50 nm. Here the nanoparticles appear dark gray in color (indicating more electron density than for the $(Si/AlO_2)Cl$ particles). The arrows indicate K_8**1**$/(Si/AlO_2)$ particles with diameters in the range of 15.8−18.5 nm, consistent with DLS measurements. (D) Enlargement of a single particle shows it to be of the average size for the sample (∼17 nm). Bar = 25 nm. Upon magnification, the presence of the electron-dense W-based POMs now becomes clear (black dots). Clumping of the K_8**1** monoanions on the surface of the $(Si/AlO_2)^{n+}$ particle is also apparent. The background texture seen in all four micrographs is due to the carbon coating on the copper grids.

$(Si/AlO_2)^{n+}$ nanoparticle (dark gray). In contrast, similar electron density is not seen on the reactant $(Si/AlO_2)Cl$ particles (light gray spheres in Figure 7A,B).[40b] A uniform distribution of K_8**1** on the surface of the $(Si/AlO_2)^{n+}$ nanoparticle is not seen in Figure 7D. Instead, the POM appears clumped on the upper left surface of the silica particle and spreads downward on a diagonal. This is consistent with some nonuniformity in the cationic sites on the Bindzil CAT nanoparticles. The size and appearance of the K_8**1**$/(Si/AlO_2)$ particles remain the same after catalysis (aerobic thioether and aldehyde oxidation data previously reported elsewhere).[2]

Cryo-High-Resolution Scanning Electron Microscopy. Samples of $(Si/AlO_2)Cl$ and K_8**1**$/(Si/AlO_2)$ were observed by cryo-HRSEM to analyze the characteristics of each in their frozen *hydrated state*. Frozen samples were etched to remove excess vitreous ice prior to imaging by cryo-HRSEM. A series of experiments were performed to determine the etching time necessary to sublime off sufficient quantities of unbound water, but not distort the fundamental silica structure.[41] The optimal etching time was determined to be 15−20 min in the 10^{-7} Torr vacuum range.

Cryo-HRSEM of colloidal suspensions of cationic silica and POM electrostatically bound to the surface of $(Si/AlO_2)^{n+}$ show uniformity in size and structural characteristics over the entire sample area at low magnification (approximately 80×; not shown). In Figure 8A, aggregates of $(Si/AlO_2)Cl$ ∼96 nm in diameter are seen and are linked together in a gelatinous network. In contrast, cryo-HRSEM images of K_8**1**$/(Si/AlO_2)$ show aggregates ∼26 nm in diameter linked by a filamentous network, indicating the initial stages of micro-gel formation (Figure 8B). The presence of these features in both samples is not surprising since colloidal silica is known to aggregate and form gels upon aging.[3] However, it is noteworthy that the K_8**1**$/(Si/AlO_2)$ sample gelled to a lesser degree over several months than the $(Si/AlO_2)Cl$. This suggests the presence of the POM (K_8**1** monoanions) retards the gelation process. Furthermore, these experiments show that cryo-HRSEM is a valuable tool for visually studying the physical properties of fresh and aged colloidal suspensions of $(Si/AlO_2)Cl$ and K_8**1**$/(Si/AlO_2)$.

Catalytic Activation of the Polyoxometalate upon Electrostatic Association. In a recent report, a dramatic increase in catalytic activity is observed when K_8**1** is bound to the surface of $(Si/AlO_2)^{n+}$.[2] EPR data of the POM alone (K_9**1**) show a high-spin ferric signal at $g = 4.30$. This signal becomes significantly more intense per POM unit and changes shape slightly upon electrostatic immobilization of K_8**1** on $(Si/AlO_2)^{n+}$ (Figure 9). Since the POM alone is nearly inactive catalytically (Table 1), one plausible explanation for this observation is that the Fe(III) centers are becoming dissociated from the rest of the POM framework upon electrostatic binding. To test this hypothesis, Fe(III) was

(40) (a) Although it appears that the POM-coated nanoparticles in Figure 7C are smaller in size than the $(Si/AlO_2)Cl$ nanoparticles seen in Figure 7A, this is due to the inability to distinguish subtle differences in the shades of gray present under the brightness and contrast levels necessary to compensate for the high electron density of the POM vs the lower and similar electron densities of the cationic silica and the carbon background at a magnification of 150000×. Therefore, the enlargements in (B) and (D) of Figure 7 are provided to allow for exact size determination. (b) An increase in electron density due to the presence of d-block metals on the surface of silica has been previously observed. Representative papers include the following: (i) Ramesh, S.; Koltypin, Y.; Prozorov, R.; Gedanken, A. *Chem. Mater.* **1997**, *9*, 546−551. (ii) Dhas, N. A.; Gedanken, A. *J. Phys. Chem. B* **1997**, *101*, 9495−9503. (iii) Eppler, A. S.; Rupprechter, G.; Anderson, E. A.; Somorjai, G. A. *J. Phys. Chem. B* **2000**, *104*, 7286−7292. (iv) Pol, V. G.; Srivastava, D. N.; Palchik, O.; Slifkin, M. A.; Weiss, A. M.; Gedanken, A. *Langmuir* **2002**, *18*, 3352−3357. (v) Pol, V. G.; Gedanken, A.; Calderon-Moreno, J. *Chem. Mater.* **2003**, *15*, 1111−1118.

(41) Wright, E. R.; Conticello, V. P.; Apkarian, R. P. *Microsc. Microanal.* **2003**, *9*, 286−295.

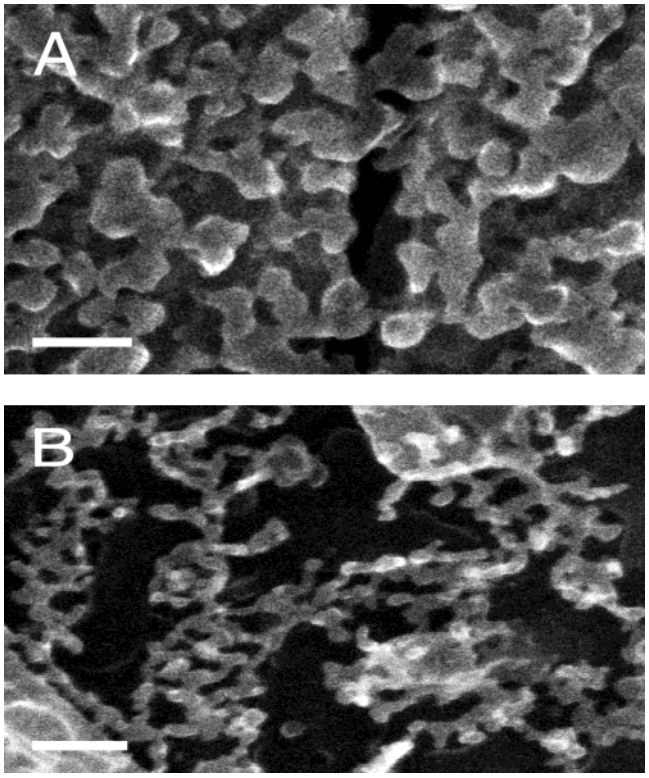

Figure 8. Cryo-HRSEM of colloidal suspensions of cationic silica ($(Si/AlO_2)Cl$) and POM nanoparticles (K_8**1**$/(Si/AlO_2)$). Both samples had aged approximately 4 months prior to imaging. (A) Cryo-HRSEM image of aged $(Si/AlO_2)Cl$ (etching time = 15 min). Bar = 200 nm. The sample is comprised of large aggregates (~96 nm in diameter) that have formed a gel. (B) Aged sample of K_8**1**$/(Si/AlO_2)$ as seen by cryo-HRSEM (etching time 20 min). Bar = 200 nm. Here the beginnings of micro-gel formation are seen with ~26-nm aggregates connected by a thin filamentous network. The presence of the K_8**1** monoanions reproducibly inhibits the gelation process.

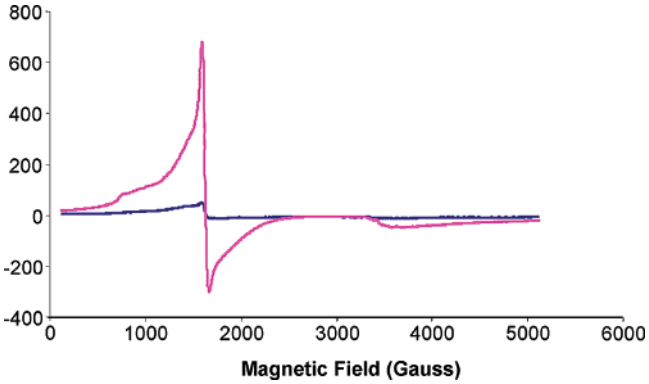

Figure 9. EPR spectra of K_9**1** (blue line) and K_8**1**$/(Si/AlO_2)$ (pink line) recorded at 6 K with a microwave frequency of 9.655 GHz and a microwave power of 20 dB. The high-spin ferric signal at $g = 4.30$ changes shape slightly and becomes significantly more intense upon electrostatic binding of K_8**1** to $(Si/AlO_2)^{n+}$.

deposited on the $(Si/AlO_2)Cl$ particles and the catalytic activity of the composite material was assessed. It was almost completely inactive (Table 1), suggesting that complete dissociation of Fe(III) from the POM in K_8**1**$/(Si/AlO_2)$ is highly unlikely. A second explanation for the increase in catalytic activity may be related to the observation that one of the nine cations of K_9**1** is lost on average upon binding to the surface of $(Si/AlO_2)^{n+}$. Since it is well-known that the formation and stability

Table 1. Aerobic Oxidation of Tetrahydrothiophene (THT) to Tetrahydrothiophene Oxide (THTO)[a]

catalyst	% conv.[b]	% yield[c]	TON[d]	TOF (h^{-1})[e]
$(Si/AlO_2)Cl$[f]	0	0	0	0
$Fe(Si/AlO_2)$[g]	1.5	1.5	1.8	0.02
$TBA_6[Fe_4(OH_2)_2(B-PW_9O_{34})_2]$[h]	0	0	0	0
$[Fe_4(OH_2)_2(B-PW_9O_{34})_2]^{6-}/(Si/AlO_2)$	2.0	2.0	4.4	0.04
TBA_9**1**[h]	2.5	2.5	2.2	0.02
K_8**1**$/(Si/AlO_2)$	28	28	60	0.5

[a] General conditions: 0.99 mmol (0.397 M) of THT, 0.875 mmol (0.35 M) of dichlorobenzene (internal standard), and the appropriate amount of catalyst containing 0.0045 mol of POM were stirred in 2.5 mL of CH_3CN under 1 atm of air at 75 °C for 120 h. [b] % conversion = (moles of THT consumed/initial moles of THT) × 100%. [c] % yield = (moles of THTO/initial moles of THT) × 100%. [d] Turnover number (TON) = moles of THTO/moles of POM. [e] Turnover frequency (TOF) = TON/reaction time (120 h). [f] 0.18 g of $(Si/AlO_2)Cl$ used. [g] Fe(III)-coated Bindzil CAT; 0.0008 mmol of $Fe_2(SO_4)_3$ (no POM present). [h] Homogeneous reaction.

of POMs derived from A-type $(PW_9O_{34})^{9-}$ units are particularly sensitive to the nature and number of countercations, it seems reasonable that an exchange of even a single K^+ cation for a $(Si/AlO_2)^{n+}$ surface site may result in subtle structural changes to the POM which result in its catalytic activation.[42-46] Isomerization from the A-type to the B-type sandwich complex is one such possible structural change. It has been previously shown that A-type sandwich complexes are unstable in aqueous solutions, converting to the B-type isomer with a number of intermediates appearing as a function of countercation.[45,47] Therefore, the possibility of isomerization to the B-type sandwich structure $[Fe_4(OH_2)_2(B-PW_9O_{34})_2]^{6-}$ was investigated by depositing this complex on the surface of $(Si/AlO_2)^{n+}$. The catalytic data in Table 1 show that both a homogeneous solution of $[Fe_4(OH_2)_2(B-PW_9O_{34})_2]^{6-}$ and the heterogeneous $[Fe_4(OH_2)_2(B-PW_9O_{34})_2]^{6-}/(Si/AlO_2)$ system are far less active than K_8**1**$/(Si/AlO_2)$, and thus it is improbable that this type of isomerization is the factor responsible for the dramatic activation seen upon POM binding.

Conclusion

The previously reported heterogeneous oxidation catalyst K_8**1**$/(Si/AlO_2)$ has been further characterized by a variety of physicochemical methods. Remarkably, three sets of titration experiments are consistent with a nonuniform distribution of charge on the surface of the $(Si/AlO_2)^{n+}$ particles and that there are 58 molecules of POM electrostatically bound to the surface of each silica particle, on average. These results not only further characterize the material but also reinforce the initial conclusions from DLS, elemental analysis, and TEM. New cryo-HRSEM experiments reveal that the presence of K_8**1** on the surface of the $(Si/AlO_2)^{n+}$ particles inhibits

(42) Kim, K.-C.; Pope, M. T. *J. Am. Chem. Soc.* **1999**, *121*, 8512−8517.
(43) Tourné, C. M.; Tourné, G. F.; Weakley, T. J. R. *J. Chem. Soc., Dalton Trans.* **1986**, 2237−2242.
(44) Tourné, C. M.; Tourné, G. F. *J. Chem. Soc., Dalton Trans.* **1988**, 2411−2420.
(45) Contant, R. *Can. J. Chem.* **1987**, *65*, 568−573.
(46) Maksimovskaya, R. I.; Maksimov, G. M. *Inorg. Chem.* **2001**, *40*, 1284−1290.
(47) Knoth, W. H.; Domaille, P. J.; Farlee, R. D. *Organometallics* **1985**, *4*, 62−68.

the thermodynamic propensity of colloidal silica to aggregate or link together by gelation, thereby forming a three-dimensional network. Additional catalytic THT oxidation experiments show that decomposition of the POM through the dissociation of the Fe(III) centers or isomerization to the B-type sandwich complex is not likely responsible for the enhancement seen in catalytic activity upon electrostatic immobilization of the POM on the surface of the $(Si/AlO_2)^{n+}$ nanoparticles.

Acknowledgment. We would like to thank the Army Research Office Grant DAAD19-01-1-0593 for support, P. Bergoo of Akzo Nobel for assistance with silica products, Kenneth I. Hardcastle for the X-ray powder patterns, NSF Grant CHE-9974864 for funding the D8 X-ray instrument, B. H. Huynh and G. Jameson for EPR, and Dr. Fredric M. Menger for use of the dynamic light scattering instrument.

Supporting Information Available: Additional experimental calculations and X-ray powder patterns. This material is available free of charge via the Internet at http://pubs.acs.org.

CM049814V